Chapter 6

Pixel Detector Improvements and Upgrades

At the heart of CMS is the silicon pixel detector [1]. It aims to provide three high-precision space point measurements to reconstruct charged particle trajectories. These three points are sufficient to produce good track information for the High Level Trigger (HLT) and for the efficient seeding of the reconstruction of longer tracks in the full tracker volume. The close proximity of the first detector layer to the interaction point (4.4 cm) minimizes multiple scattering effects and extrapolation uncertainties making the pixel information crucial for the reconstruction of the initial position and direction of the charged tracks. The pixel detector therefore plays a key role in the identification of primary vertices, secondary vertices, and secondary tracks. These elements are essential for the efficient identification of long lived particles, such as b quarks, and for the search for new physics at the LHC.

The present CMS pixel detector was conceived over 10 years ago and designed for a maximum luminosity of $1 \times 10^{34}\,\mathrm{cm}^{-2}\mathrm{s}^{-1}$. Following the Phase 1 upgrade of the LHC, the peak luminosity is foreseen to reach $2 \times 10^{34}\,\mathrm{cm}^{-2}\mathrm{s}^{-1}$ before the next long shutdown. The present pixel system will not be able to sustain such extreme operating conditions due to large data losses in the read out chip (ROC) and must be replaced in the long shutdown of 2016. This is the best, and perhaps only, opportunity to install and commission a new system before the luminosity will exceed $1 \times 10^{34}\,\mathrm{cm}^{-2}\mathrm{s}^{-1}$. The modular design of CMS allows good access to the pixel system, which can be extracted relatively easily, independently of the beam pipe or the strip tracker.

The baseline plan presented here is to replace the current system with an ultra-light pixel detector, with improved ROCs, having four barrel layers and three end-cap disks. The conceptual layout for the Phase 1 pixel detector is shown in Figure 6.1. The addition of the fourth barrel layer at a radius of 16 cm and the third forward disks will maintain the present level of tracking performance even in the high occupancy environment of the upgraded LHC. In addition, it provides a safety margin in case the first silicon strip layer of the Tracker Inner Barrel (TIB) degrades more rapidly than expected.

This upgrade of the pixel system will address all of the following shortcomings of the current detector:

- The most severe limitation is the ROC, which is just adequate at the LHC design luminosity of $1 \times 10^{34}\,\mathrm{cm}^{-2}\mathrm{s}^{-1}$. At this luminosity, buffer size and readout speed limitations are estimated to produce a dynamic inefficiency of 4% ($> 16\%$) if the bunch spacing time is 25 ns (50 ns). The dynamic inefficiency increases exponentially with increasing luminosity. At $2 \times 10^{34}\,\mathrm{cm}^{-2}\mathrm{s}^{-1}$ and 25 ns bunch spacing the ROCs in the inner region will suffer an inefficiency of 15%, leading to a major degradation of the overall level of tracking performance.
- The three-hit coverage of the detector is not completely hermetic, leading to 10-

DRAFT

15% inefficiencies at $|\eta| < 1.5$ and larger track seeding inefficiencies in the region $1.5 < |\eta| < 2.5$. This limits the efficiency of HLT tracking triggers and slows the full tracking algorithm. The situation will degrade even further at higher luminosities.

- The radiation hardness of the detector is not sufficient for operation up to the end of Phase 1, when the integrated luminosity will be around 350 fb^{-1}. Although the detector was constructed using the most radiation resistant technology known at the time of its fabrication, radiation damage will degrade its performance and necessitate replacement of the inner regions.
- The detector contains significant passive material that degrades tracking and calorimetric measurements due to multiple scattering, photon conversions and nuclear interactions.

The goal of the Phase 1 upgrade is to provide a pixel detector that can maintain a high efficiency at a luminosity of $2 \times 10^{34}\,cm^{-2}s^{-1}$, with less material, and will provide 4 hits over pseudorapidities up to 2.5. In the years since the design of the current detector, innovations in cooling, power distribution, mechanical support, CMOS electronics, and sensor materials enable the construction of a significantly more performant detector.

Radiation damage is still expected to significantly degrade the performance of the innermost regions during the three year Phase-1 run beginning in 2017. The position resolution of the detector will worsen by roughly a factor two after a fluence of $10^{15} n_{eq} cm^{-2}$. The dynamic inefficiency is expected to be greater during the second half of this run as the luminosity increases. We are therefore considering the development of replacement parts based on smaller pixels, a more radiation-resistant sensor technology, and an improved readout chip based on a denser CMOS technology. The replacement would occur near the middle of the run and would ensure that detector performance increases rather than decreases during the period when the largest data samples are being acquired.

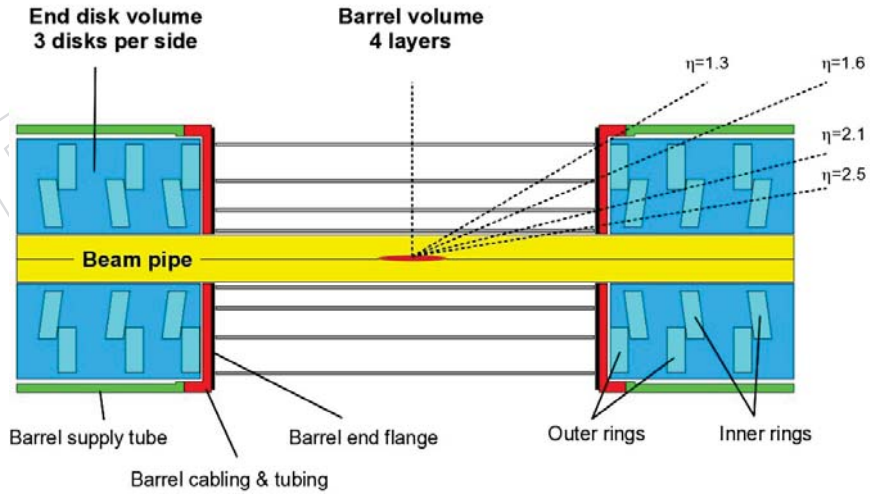


Figure 6.1: Schematic view of the Upgrade Layout. It consists of four barrel layers and three endcap disks on each side, with each disk separated into an inner and outer ring. The disks are placed in locations so as to maximize the 4-hit η coverage.

The implementation of the Phase 1 pixel detector would largely improve all aspects of CMS tracking:

- The addition of the extra layers will dramatically improve the efficiency and resolu-

tion of pixel-only tracks. Pixel tracks are a crucial part of the HLT and they are also used to seed the full tracking, leading to an increase of the efficiency and a decrease of the fake rate for full tracks.

- The decrease in the amount of material and the increase in the number of measurement points improve the resolution of all track parameters. In particular, the resolution of longitudinal and transverse impact parameters are significantly improved.
- The efficiency and resolution enhancements lead to much improved primary and secondary vertexing. Vertexing is essential to associate the final state particles with the correct primary vertex in the high pile-up LHC environment. Secondary vertexing plays a key role in b-tagging and the search for various long-lived exotic states.
- The improvements in tracking efficiency, fake rate, parameter resolution, and vertexing all contribute to significant improvements in the b-tagging performance of the tracker. The b-tagging performance for the present and upgraded detectors is shown in Fig. 6.2 for operation at an instantaneous luminosity of $1\times10^{34}\text{cm}^{-2}\text{s}^{-1}$ with 25 ns bunch spacing. The upgraded detector would reduce the light quark background of the Combined Secondary Vertex Tag by a factor of 6 for a b-efficiency of 60%, or conversely, it would increase the b-quark efficiency by approximately 50% at the fixed light-quark efficiency of 5×10^{-2}.

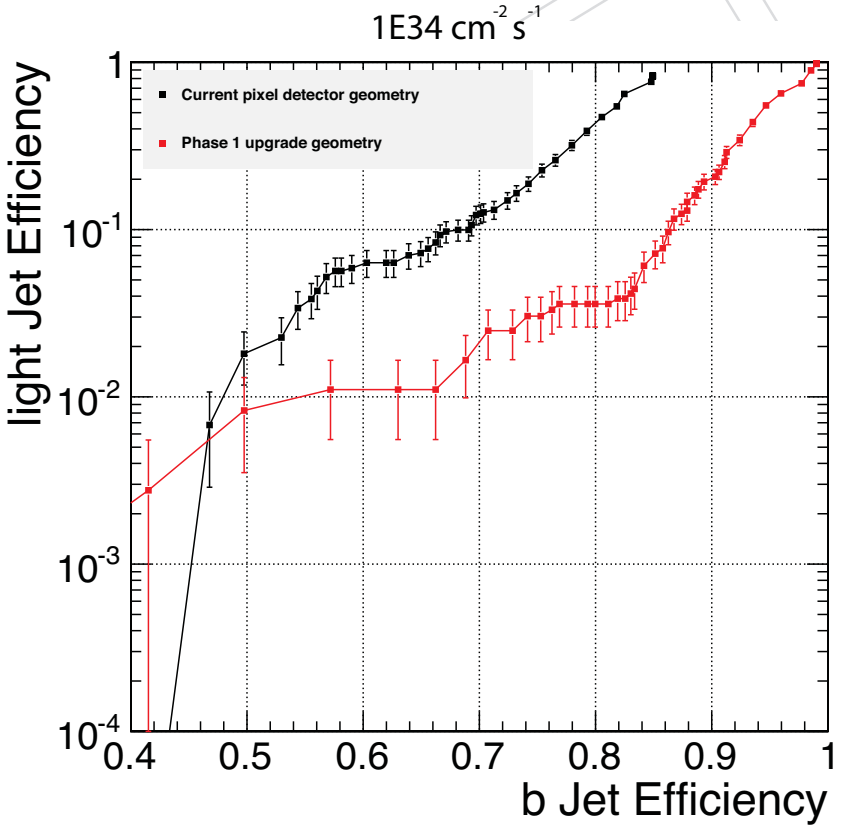


Figure 6.2: The light quark and b quark efficiencies of the Combined Secondary Vertex b-tagging algorithm are shown for the present and upgraded detector (with inner radius of 3.9 cm, 285 μm thick sensors and $100\times150\,\mu\text{m}^2$ pixels) at an instantaneous luminosity of $1\times10^{34}\text{cm}^{-2}\text{s}^{-1}$ with 25 ns bunch spacing.

In this chapter we outline the basic performance characteristics of the current pixel detector. We also point out some of the factors that limit its performance, and describe the proposed improvements to the mechanics, layout and electronics which would significantly enhance our physics capabilities during the first stages of the major upgrades to the LHC. This upgrade to the pixel detector significantly improves charged particle tracking for CMS and greatly enhances the experiment's physics reach during the crucial Phase 1 upgrade to the LHC when a large fraction of the luminosity will be delivered.

6.1 Performance of Current Detector

In this section, we discuss in more detail the performance of the current pixel detector and enhancements that the proposed detector upgrade will provide.

6.1.1 Electronics and Readout

The current pixel readout electronics were designed and optimized for the data rates and pixel occupancies expected up to the LHC design luminosity of $1 \times 10^{34}\,\mathrm{cm}^{-2}\mathrm{s}^{-1}$. There will be a dynamic inefficiency of about 4% from the current readout chip, PSI46v2, at this luminosity in the innermost layer. These losses are shown in Figure 6.3 as a function of the level-1 trigger accept (L1A) rate as measured in test beam runs with particle fluxes as expected for LHC design luminosity [2]. At the nominal L1A accept rate of 100 kHz, the data loss will increase to 16% in the innermost layer as the luminosity goes up by a factor of two (for 25 ns bunch crossing) to $1 \times 10^{34}\,\mathrm{cm}^{-2}\mathrm{s}^{-1}$. These losses are understood by simulations and characterizations of the PSI46v2 readout chip to be coming from two sources: the column drain dead time (0.8%) and readout-related losses (3.0%). Hit pixels are transferred using column drain readout to the chip periphery where the hits are stored in buffers during the L1 trigger latency (3.2 μs). If instead the LHC runs with 50 ns bunch spacing at $2 \times 10^{34}\,\mathrm{cm}^{-2}\mathrm{s}^{-1}$, then the data losses continue to increase almost exponentially, with losses on the order of 50% for the innermost layer for example.

Figure 6.4 illustrates the impact on performance of charged particle tracking from these data losses. In these simulated $t\bar{t}$ events at instantaneous luminosities of $2 \times 10^{34}\,\mathrm{cm}^{-2}\mathrm{s}^{-1}$ with 25 ns bunch spacing, we see substantial decreases in the tracking efficiency. These high luminosities also lead to a large fake rate even without the previously mentioned data losses. The degradation with 50 ns bunch spacing would be substantially worse. The conclusion is that the current readout chip is not able to cope with these rates in the innermost layers of the pixel detector.

In the present operation of the pixel detector events are observed with much higher pixel hit counts than expected from minimum bias event simulations. They are attributed to beam-gas collisions with charged tracks going almost horizontally through the barrel layers. These events can cause problems at the system level including the loss of event synchronization. By now, beam-gas events can largely be suppressed in the readout by excluding certain background triggers. However, the rate of these events scales with beam intensity and hence it could become more problematic in the future when we have to deal with high numbers of multiple collisions. Changes to the readout chip and downstream electronics would be one course of action to alleviate these problems.

6.1.2 Sensor Radiation Hardness

At the design luminosity of $\mathcal{L} = 10^{34}\,\mathrm{cm}^{-2}\,\mathrm{s}^{-1}$ the pixel system will be exposed to particle fluences of 3×10^{14}, 1.2×10^{14}, and 0.6×10^{14} $\mathrm{n}_{eq}/\mathrm{cm}^2/\mathrm{yr}$, at the first, second, and third layer,

DRAFT

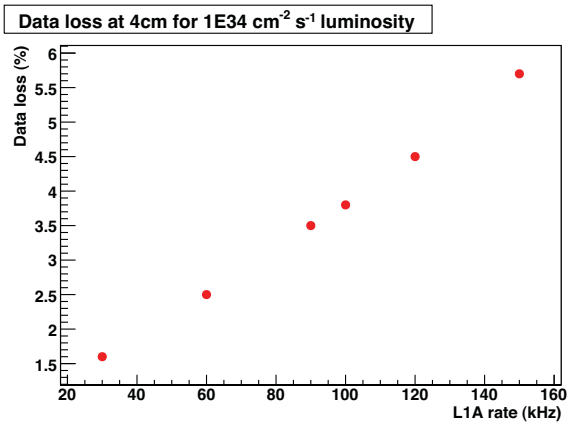


Figure 6.3: Left: Data losses as a function of the L1 accept rate of the innermost layer of the current pixel detector [2]. The instantaneous luminosity is 10^{34} cm^{-2}s^{-1} and the bunch spacing is 25 ns. CMS has been designed for maximum average L1 trigger rates of 100 kHz. The data points beyond this rate in the plot simply illustrate the linear nature of this data loss at this particular instantaneous luminosity with the PSI46v2 readout chip.

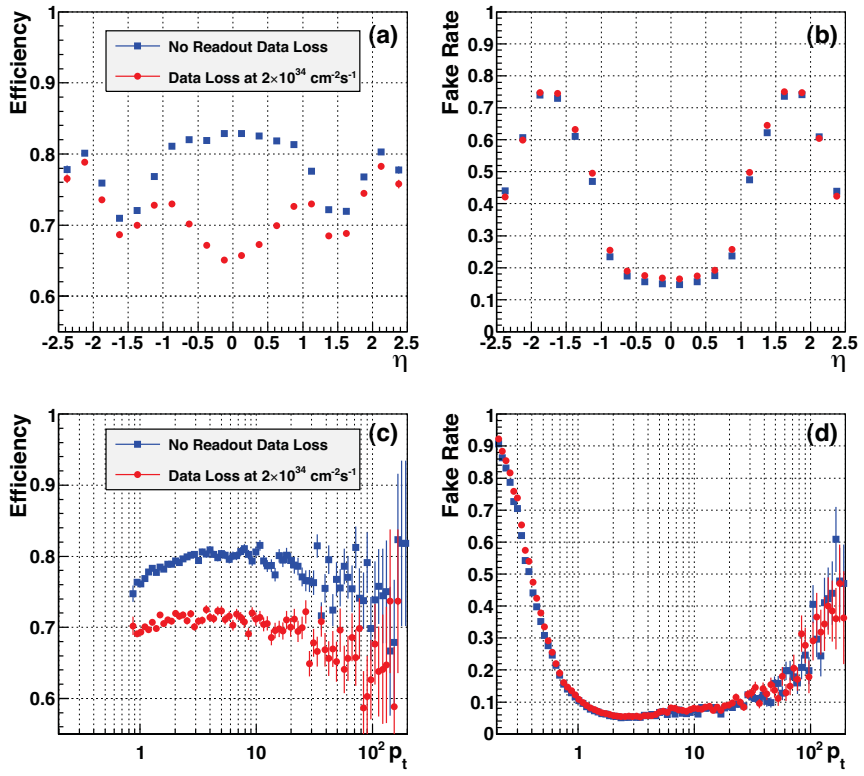


Figure 6.4: Performance of the current pixel detector in $t\bar{t}$ events at 2×10^{34} cm^{-2}s^{-1} with no data loss (blue) and with the estimated data loss from buffer overflows mentioned in the text (red): (a) tracking efficiency vs pseudorapidity; (b) fake rate vs pseudorapidity; (c) efficiency vs p_T; (d) fake rate vs p_T.

respectively. Fluences for the endcaps are comparable at the same radii. All components of the current system are specified to operate up to a total particle fluence of at least 6×10^{14} n_{eq}/cm^2. The sensors for BPIX and FPIX have been developed to operate efficiently up to this dose. They are n^+-on-n (n^+ implants on n bulk silicon) devices [3]. Electron collection has the advantage that after radiation-induced space charge sign inversion, the highest electric field is located close to the collecting electrodes, so even when the detector is not fully depleted after radiation damage, the depletion zone is near the side that is read out. Moreover, since electrons have larger mobility and consequently a lower trapping probability than holes, electron collection leads to a higher charge collection efficiency (CCE) after irradiation.

Studies of the radiation damage effects on the performance of both the BPIX and the FPIX sensors have been performed. The barrel-type pixel sensors with their readout chips have been exposed to radiation fluences up to 5×10^{15} n_{eq}/cm^2 [4–6]. Charge collection of signals have been measured as shown in Figure 6.5. After a fluence of 1.1×10^{15} n_{eq}/cm^2 only about 50% of the charge is collected for $V_{bias} > 400$ V.

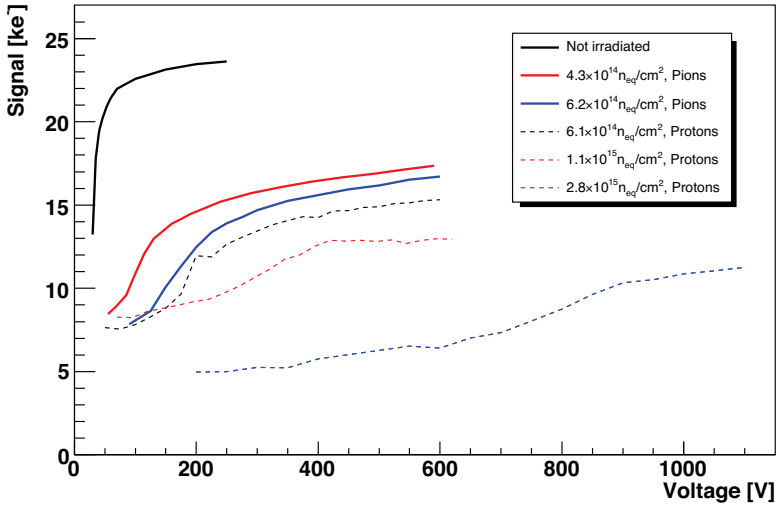


Figure 6.5: Most probably value of signal charge collected from single clusters as a function of the sensor bias for various irradiation fluences of barrel pixel sensors [4]. (It should be noted that biasing the sensor to 1000 V is not considered feasible with the actual detector and power supplies.)

Hit detection efficiency and resolution is expected to deteriorate with irradiation. For a radiation fluence above 10^{15} n_{eq}/cm^2 the hit efficiency measured in beam tests is below 97%. Figure 6.6 shows the simulated hit resolution as function of the track pseudorapidity before and after irradiation. The fluence 1.2×10^{15} n_{eq}/cm^2 is expected to be exceeded during Phase 1. After this exposure, the detector's hit resolution deteriorates by roughly a factor of two in the transverse plane and would require a replacement of the innermost layer. The Phase 1 upgrade pixel detectors must be designed to facilitate this partial replacement. This presents an opportunity to adopt more radiation hard sensors, if they can be developed in time.

6.1.3 Material In the Tracking Region

The services (including cables, cooling lines, printed circuit boards) and mechanical support structure (e.g. end flanges) for the current pixel detector introduce a non-negligible amount

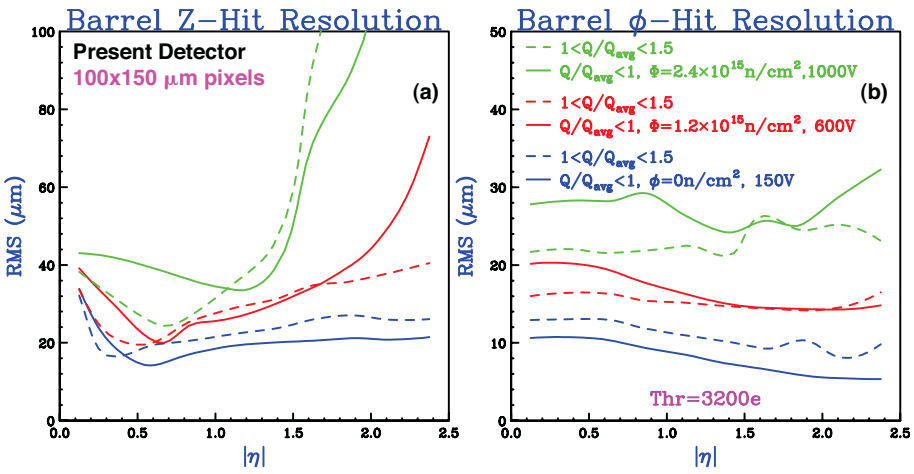


Figure 6.6: Hit position resolution (RMS) as function of the track pseudorapidity for an unirradiated (blue lines) and irradiated detectors (red and green lines). Longitudinal (a) and transverse hit resolution (b) are show separately. The solid lines correspond to hits with total charge Q below the average charge. Dashed lines correspond to hits with total charge $1 < Q/Q_{avg} < 1.5$.

of material in the tracking volume. This reduces the track reconstruction efficiency and degrades the impact parameter resolution. The material distribution of the current pixel detector is shown in Figure 6.7 in terms of radiation lengths and nuclear interaction lengths as function of η.

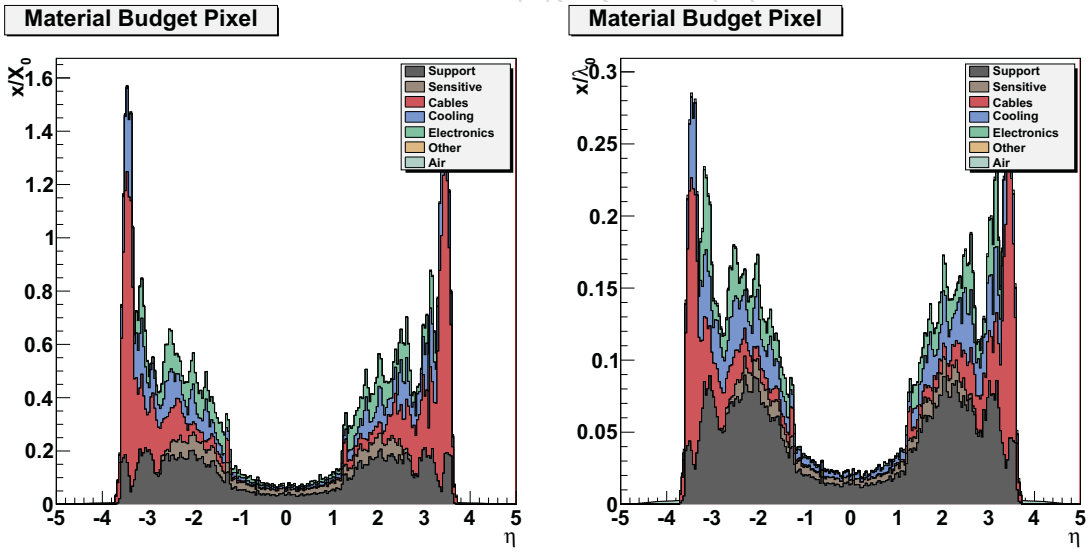


Figure 6.7: Radiation length (left) and nuclear interaction length (right) of current pixel detector.

Figure 6.8 shows the location of various parts and components for the current pixel detector along the z-direction. For BPIX, all the power and signal cables are routed to two end-flanges, behind both ends of the barrel region, and then directed to an optical link system that converts the electrical signals into optical. The signal is then sent over a 2 m long optical fiber to the patch panel on the tracker bulkhead. In the central region ($|\eta| < 1.2$), the main contribution to the

total amount of material comes from the silicon sensors, the chips, the mechanical structure, cooling pipes, and Kapton flex cables. For $|\eta| > 1.2$, before getting to the FPIX, the main contributions are due to the cooling manifolds, the PCB end-flange print with more than 800 plugs and the Kapton cables. In addition, the cooling manifolds and the PCB end-flange are directly in front of the first forward disk of the FPIX system. Most of the material between $1.2 < |\eta| < 2.4$ is in the FPIX disks (brazed aluminum cooling loops) and electronics (ZIF connectors and adapter boards), and between $2.4 < |\eta| < 3.6$ in cables and cooling.

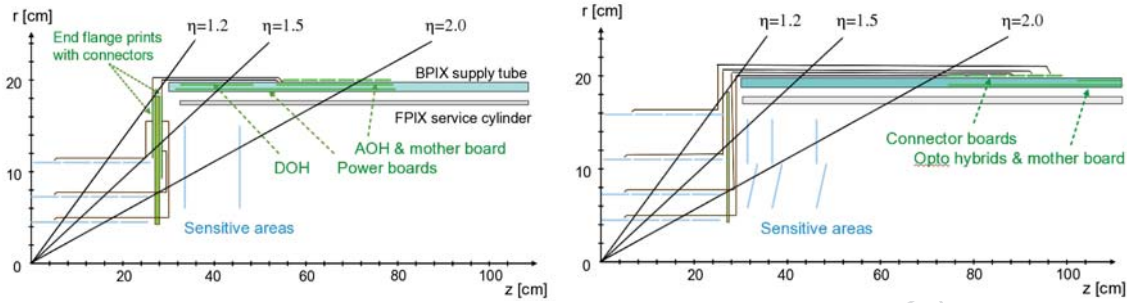


Figure 6.8: Location of components as a function of z and η for the current pixel detector (left), and for the proposed upgraded detector (right). In the current detector, there are a substantial number of connectors and electronics boards in the tracking volume, in particular at the end flange between the BPIX and FPIX. These have all been moved further downstream in z in the new design.

The passive material plays a visible role for tracks with low and intermediate momenta, as illustrated in Figures 6.9 and 6.10, which show the impact parameter resolutions as measured in recent collision data, compared to simulation, versus track η and ϕ [7]. At low momenta the transverse impact parameter resolution worsens at higher η due to the material traversed by the track. The impact of the 18 cooling pipes is clearly visible for lower momentum tracks versus ϕ.

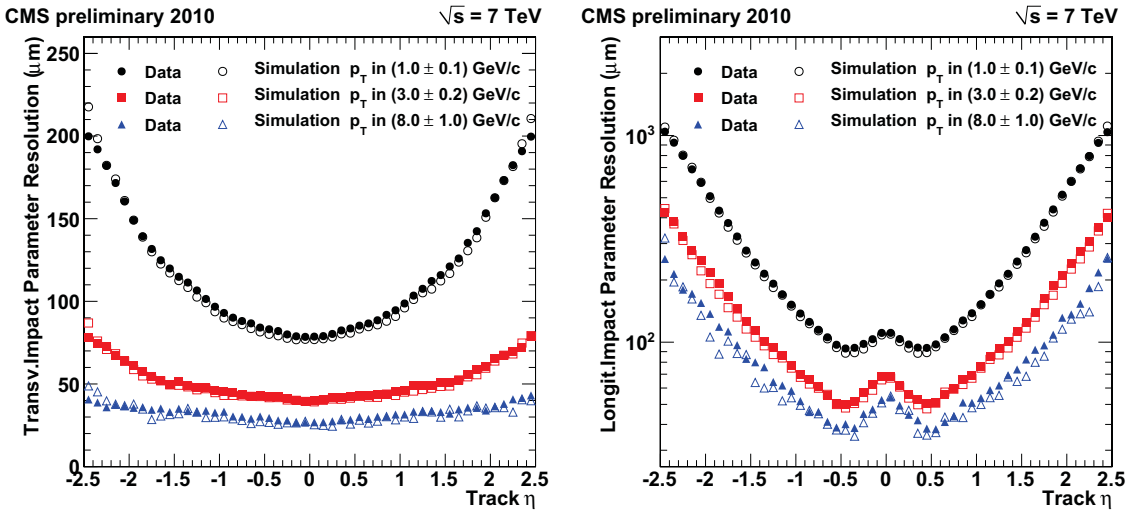
6.2 Description of the Pixel Detector Upgrade

The design of the pixel detector must satisfy the following requirements and constraints:

- Minimize data loss due to latencies and limited buffering in high luminosity running;
- Minimize degradation due to radiation damage;
- Optimize detector layout for 4-pixel-hit coverage over the η range with minimal innermost layer radius;
- To reduce material, adopt two-phase CO_2 cooling and light-weight mechanical support, moving the electronic boards and connections out of the tracking volume;
- To reuse the current patch panel and off-detector services (cooling pipes, cables and fibers), adopt DC-DC power converters and higher bandwidth electronics;
- Reduce number of module types and interfaces;

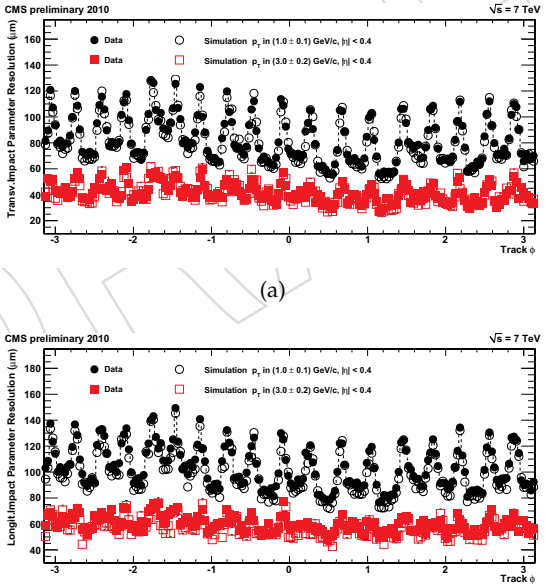
The objective is to have the system installed and commissioned during the 2016 shutdown. In this section we describe our progress, as well as some of the R&D needed for the Phase 1 upgrade and how it relates to future upgrades.

DRAFT



(a) (b)

Figure 6.9: Measured resolution of the track transverse (a) and longitudinal (b) impact parameter as a function of the track η for transverse momenta in $1.0 \pm 0.1\,\text{GeV}/c$ (circles), in $3.0 \pm 0.2\,\text{GeV}/c$ (squares) and in $8.0 \pm 1.0\,\text{GeV}/c$ (triangles). Filled and open symbols correspond to results from data and simulation, respectively [7].



(a)

(b)

Figure 6.10: Measured resolution of the track transverse (a) and longitudinal (b) impact parameter as a function of the track ϕ for transverse momenta in $1.0 \pm 0.1\,\text{GeV}/c$ (circles) and in $3.0 \pm 0.2\,\text{GeV}/c$ (squares). Filled and open symbols correspond to results from data and simulation, respectively [7]. The 18 peaks correspond to the 18 cooling structures in the BPIX as described in the text.

6.2.1 Geometrical Layout

For the Phase 1 upgrade of the CMS detector, we propose a pixel detector with 4 barrel layers and 3 disks in each endcap. The 4 barrel layers are of equal length and are placed at radii of 3.9, 6.8, 10.9, and 16.0 cm. The three end-cap disks are placed on each side of the central barrel detector, with a radial coverage ranging from 4.5 to 16.1 cm. The location of the first disk along the beam line is at 29.1 cm from the interaction point, the second and third disks are located at 39.6 cm and 51.6 cm from the interaction point.

In the new design, there will be only one type of module with 16 readout chips in a 2×8 arrangement. They will be mounted on ultra-lightweight support structures integrated with the cooling distribution system. Two-phase CO_2 cooling will replace the current single phase C_6F_{14} resulting in significant material reduction. We plan to use thin-walled stainless steel pipes with a diameter of about 1.6 mm and wall thickness of 0.1 mm which will provide enough cooling power for each pixel sub-assembly based on a continuous loop. Further material reduction will be achieved by using longer twisted pair or light-weight flex-cables to carry the signals to the optical hybrid boards; these boards, as well as the port cards and cooling manifolds, will be moved out of tracking region.

The outer and inner parts of the detector will be designed such that they would allow the inner layers and rings to be easily replaced after radiation damage. For FPIX, this requires each half-disk be divided into an inner and outer ring. Figure 6.1 shows a cross-sectional view of the new pixel system and its sections. Similar to the current detector, the blades in the forward disks are rotated by 20° in a turbine like geometry to induce charge sharing. The separation of each half disk into an inner and outer assembly allows us to optimize the orientation and tilting to obtain the best position resolution in both radial and ϕ directions. Our baseline is to tilt the inner assemblies into an inverted cone at 12° towards the interaction point.

The upgraded pixel detector is constrained by the existing insertion volume and services. The cabling of the current CMS tracker detector, which includes the 200 m^2 silicon strip detector, was facilitated by the installation of two patch panels, denoted as PP1 and PP0, outside the tracker volume. This infrastructure will not be changed during the Phase 1 upgrade except for the cooling pipes between PP0 and PP1. Therefore, the upgraded pixel detector must use the existing power cables, fibers, and cooling lines from the cooling plant to PP1. Cables, fibers, and other required utilities are already installed up to PP0 for 3 forward disks; however, space for making changes to utilities between PP1 and PP0 is severely limited. The existing rail system for insertion and extraction will be used.

6.2.2 New Beam Pipe

To improve the physics performance of a pixel detector in terms of impact parameter resolution and vertex resolution the first active layer should be as close as possible to the beam, requiring a beam pipe of minimum possible radius. This requirement has to be balanced against the safe and efficient operation of the accelerator with minimum background in the experiment. For the safety of the detector, the last machine element in the interaction region should always be the point of smallest aperture. In addition, the minimum diameter is constrained by mechanical stability under vacuum. The CMS beam pipe spans over ±18 m from the interaction point to both ends of the experimental cavern. It is segmented into a central section and 4 sections on each end. The central section is 6.2 m long and consists of a cylindrical part of 1.8 m length and conical ends. The cylindrical piece is made out of 0.8 mm thick beryllium; the conical parts are of 0.8-1.2 mm thick stainless steel. The inner diameter at the interaction point is 58 mm.

DRAFT

The LHC machine group has studied the beam aperture for the LHC upgrade scenario. It was concluded that changing the minimum diameter of the central part of the CMS beam pipe from 58 mm to 50 mm will not cause any aperture problems in the CMS interaction region, provided all tolerances can be controlled to 11 mm. Therefore, it is proposed to install a new central beam pipe with an inner diameter of 50 mm together with the new pixel detector. The smaller beam pipe diameter allows the reduction of the first barrel layer radius from 4.4 cm to about 3.9 cm. A further reduction to 3.4 cm is under study. The opening angle of the conical part of the beam pipe will be preserved. The cylindrical part will be shorter by about 28 cm on each end. There are two options for building the pipe. Either the conical part is again made out of stainless steel, leading to a shorter beryllium section, or we maintain the length of the cylindrical part of the beryllium section and connect the stainless steel section onto the conical beryllium ends. Detailed background studies have to be performed to judge the possible effect of a shorter beryllium section. The other solution, though in principle possible, is much more complicated from the production point of view. For both solutions detailed calculations using FEM have to be done to estimate the mechanical strength and the deflection. Also, the vacuum performance and the beam impedance have to be re-evaluated for the smaller radius.

6.2.3 Mechanical Support for BPIX

A comparison of the current 3-layer barrel and the new 4-layer system is shown in Figure 6.11. The addition of the fourth layer reduces significantly the gap between the pixel detector and the TIB. The BPIX mechanical support structure consists of 200 μm thick carbon fiber ladders, with cut-outs to reduce mass, glued onto the stainless steel cooling tubes. Each ladder is glued to two tubes. The end flange is made also of carbon fiber glued onto 4 mm thick Airex foam profiles. The bends of the tubes are made from 1.8 mm diameter 100 μm thick stainless steel soldered to the straight section. Figure 6.12 shows the prototype of the layer 1 mechanical structure.

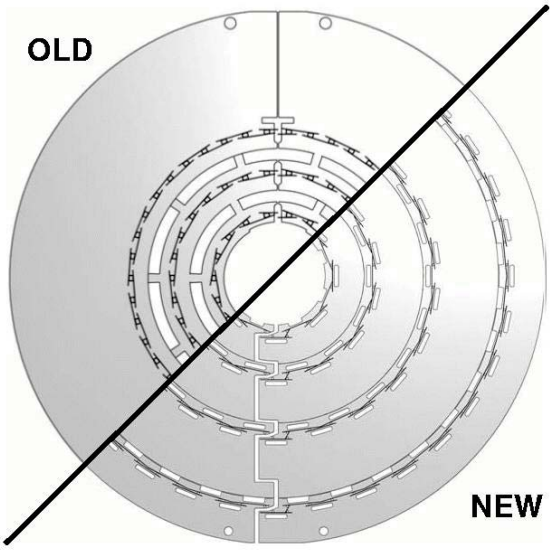


Figure 6.11: Cross sectional view of the old 3 layer barrel (top) and the new 4 layer system (bottom).

The electronic components of the services are moved to the forward direction, away from the active tracking region. The PCBs on the supply tubes are moved to $|\eta| > 2$ and those on the end flange have been removed entirely (see Figure 6.8). This has been made possible by

the development of the low mass micro-twisted pair cables described later. Modules are now connected directly to the readout optical hybrids (ROH) which are about 1 m away. A new supply tube has been designed (see Fig. 6.13) to provide optimal η coverage between BPIX and FPIX. A prototype has been built, made out of carbon fiber ribs, panels, and tubes as well as Airex foam. The total weight of the supply tube is 2900 g.



Figure 6.12: Prototype of the mechanical structure for the innermost layer. To illustrate its lightweight, a carbon fiber ladder is laid upon the half-barrel. The mechanical stability of the ladder is given by the cooling tubes.

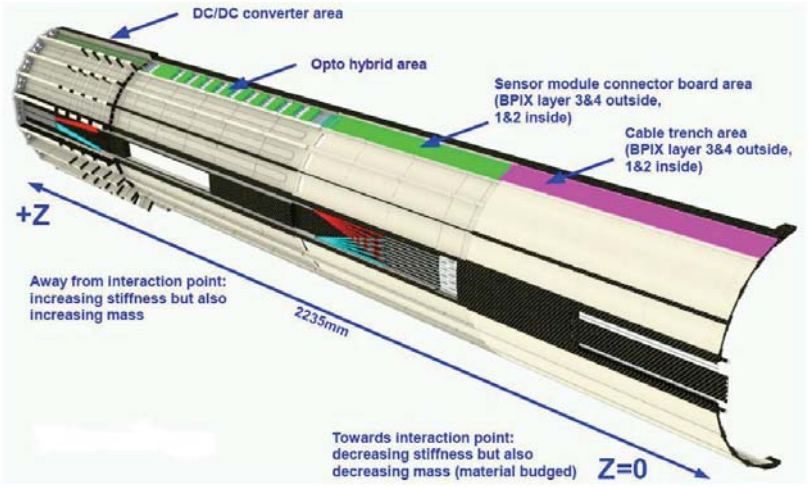


Figure 6.13: Schematic drawing of the new BPIX supply tube.

6.2.4 Mechanical Support for FPIX

The current FPIX detector has 7 module types on beryllium panels placed between $r = 59.7$ mm to 144.6 mm (there are a total 84 modules per half disk, or 540 ROCs per half disk). The upgrade layout uses only one module type (2x8 ROCs) arranged radially on panels placed between $r = 45$ mm to 161 mm (there are a total 56 modules per half disk, or 896 ROCs per half disk). Half-disks are divided into an outer ring with 34 modules and inner ring with 22 modules. The inner assembly is supported off the outer assembly by some rods and the two assemblies can be easily separated. The pixel modules are attached by a module holder to the substrate and are removable and replaceable without disassembling half-disks.

All the outer radius sensors are located to minimize the gap in 4-hit coverage between the end of the 4th-barrel layer and the innermost disk. The design maximizes the 4-hit coverage

between the end of 4th barrel layer up to $|\eta| = 2.5$, for particles originating at the IP ± 5 cm, using a minimum number of modules.

Each blade will have one module placed on opposite sides of the same substrate (see Fig. 6.14). The radial orientation of the rotated turbine aligns the 150 μm dimension of each pixel in the radial direction and the 100 μm dimension in the ϕ direction, with more overlap between neighboring sensors than in the current design. This will ease the spatial alignment for track reconstruction. We plan to use thermal pyrolytic graphite (TPG) for the substrates. TPG is a material with excellent in-plane thermal conductivity. The stainless steel cooling tubes for CO_2 cooling are embedded in the outer and inner assembly rings made out of light-weight carbon-carbon (C-C) material as shown in Figure 6.15.

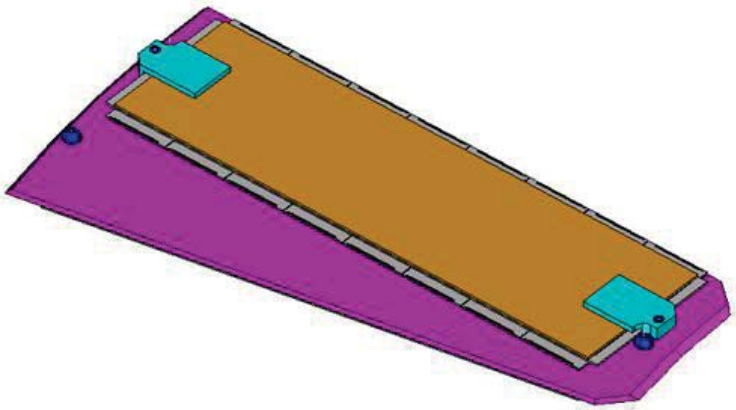


Figure 6.14: FPIX Upgrade Blade - identical blades are used in the inner and outer assemblies of all half disks.

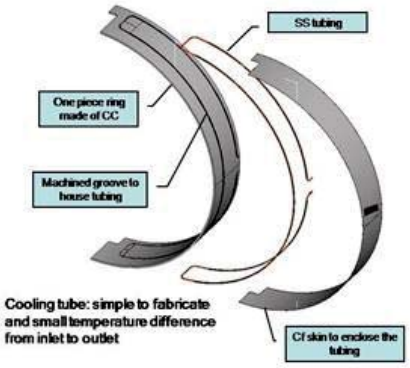


Figure 6.15: Edge Cooling Concept: cooling tube captured inside carbon-carbon ring with carbon fiber skins.

The design of the FPIX Upgrade blade is shown in Figure 6.14. It features:

- Solid TPG (0.68 mm thick) encapsulated with carbon-fiber facings (0.06 mm thick).
- All blades are identical with one 2×8 ROCs module mounted on each side.
- Each module has a pair of module holders made out of G9 glued at each end for attachment to the precision holes on the substrate.

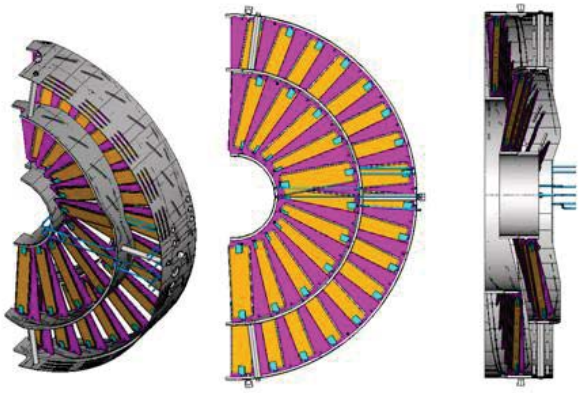


Figure 6.16: FPIX Upgrade half-disk design: Inner Blade assembly supported by Outer Blade assembly, with all blades attached permanently to the C-C assembly rings.

- Cooling is provided at the end(s) of the blade by contact with the actively CO_2 - cooled ring(s).
- Each substrate is glued permanently to the rings so that the whole ring and substrate assembly with embedded cooling tubes could be constructed as a complete structure.

Figure 6.16 shows the complete half disk, with the inner assembly ring supported by the outer assembly ring.

6.2.5 CO_2 Cooling

In the present pixel detector, cooling pipes, manifolds, heat exchanger contacts and the C_6F_{14} coolant itself represent a major contribution to the overall detector material in the Tracker acceptance. CO_2 two-phase cooling has been identified as the most promising option to improve upon the present mono-phase fluorocarbon system, in order to achieve enhanced cooling performance with a lightweight system. CO_2-based cooling has been successfully adopted in other detectors, notably the LHCb VELO.

In general, CO_2 offers significant advantages compared to mono-phase fluorocarbon:

- Excellent thermodynamic properties for small channels: low mass, less viscosity, low liquid/vapor density ratio, low dT/dP, high heat transfer coefficient, and high latent heat;
- A factor of ~ 2 lower density, in liquid phase;
- At ~ 1 CHF/kg, it is substantially cheaper than C_6F_{14} (~ 100 CHF/kg).

The high heat transfer coefficient allows smaller heat-exchanger contacts. The high latent heat allows more heat load per channel, possibly reducing needs for manifolding and the size of the manifolds, as well as the size of the individual pipes. CO_2 also offers the required radiation hardness.

The development of the CO_2 cooling system for the pixel detector requires a substantial R&D program, covering the three main areas discussed below.

1. **Characterization of heat transfer.** The pixel detector cooling uses miniature pipes involving a domain of CO_2 heat transfer and two-phase flow for which very little experimental

DRAFT

measurements exist, and available theoretical models do not give reliable predictions. A fundamental research line consists in performing laboratory measurements to characterize the process in the relevant domain, and improve the existing theoretical models accordingly.

2. **Optimization of the on-detector cooling.** The optimization of the on-detector part of the cooling system is the key to reduce the detector material, and hence achieve the required improvement on its performance. The heat transfer from the silicon sensors to the structure, through the pipe walls into the coolant has to be maximized, while minimizing the amount of material and at the same time ensure reliable thermal joints with reproducible performance. The crucial aspects are the choice of the pipe material and size, pipe fittings and connection techniques, design of thermal joints and choice of thermally conductive materials.

3. **System design and integration in CMS.** Many aspects have to be addressed, including: (i) design of the cooling station, choice of the active components and of the accumulator; (ii) design of the control and monitoring system, choice of the instrumentation (especially of the active parts that will have to be installed in the experimental cavern), interface to the detector monitoring system; (iii) design of the cooling channels between PP0 and PP1 and choice of dielectric fittings in PP1; (iv) connection to existing cooling pipes from PP1 to the cooling station, and re-qualification of the pipes; (v) interface with surroundings in the UX cavern and with the main chiller in the US cavern; (vi) optimization and validation of system operation, including startup at warm temperature, study of safety issues and failure modes.

The first area of research is already well advanced, with several labs performing measurements in parallel on different setups. A large amount of data have been collected, analyzed and carefully compared, providing evidence that a suitable phase-space of working parameters is available, compatible with performance requirements and system constraints.

The optimization of the on-detector cooling is also advancing well; prototypes of mechanical structures of both BPIX and FPIX have already been tested with CO_2 cooling in realistic conditions, and extensive thermal modelling studies are underway. Although substantial optimization work is still to be done, the results collected so far indicate that suitable performance can be achieved with miniature pipes and lightweight contacts.

System design and integration studies will be a main focus for the coming 1-2 years. A full-scale system has been built in the CERN CryoLab, and will be used as test setup to qualify components for the cooling plant as well as the control and monitoring system; it will be also used to study system aspects with long pipe runs mimicking the geometry of the CMS service channels. Preliminary safety studies indicate that the installed pipes are compatible with the required operating pressure. Excellent progress has been made in updating as-built models of the existing cooling system and of the cavern infrastructure, which are the basis of the studies for the integration of the system in CMS.

6.2.6 DC-DC Conversion

The routing and installation of the current pixel detector's services (power cables, fibers, cooling lines) was a major technical challenge. Due to the space constraints of the conduits and other sub-detectors, it would be quite difficult to route additional power cables. The pixel upgrade will increase by about a factor of two the number of ROCs. Therefore, more power will be needed than in the current detector, supplied at a higher current. To limit resistive losses

DRAFT

in the $\sim$ 50 m long power cables, a novel powering scheme based on the DC-DC conversion technique is proposed. The idea is to bring the power into the detector at a higher voltage but at a lower current (thereby significantly reducing the power losses in the cable) and to use a DC-DC buck converter close to the detector to convert the input voltages to the operation voltages needed by the pixel modules with high efficiency ($\sim$ 80%). A separate converter is used for the digital and analog voltages. These converters need to be tolerant of both the radiation and magnetic field inside the tracker volume. Since commercial converters could not satisfy these requirements, a dedicated ASIC development is needed. A prototype is currently being developed. The DC-DC conversion chip and other components will be assembled on a small printed circuit board which will be placed on the support half cylinder, close to the pixel modules. Prototypes of these converter PCBs have been fabricated and tested for electromagnetic noise emissions in a set-up with silicon strip modules. The results of these tests are promising and indicate that the application of DC-DC converters in the pixel system should be feasible.

Tests are ongoing to study the performance of pixel modules powered by the same CAEN power supply modules currently in use and with the long power cables needed by the experiment with and without DC-DC conversion. As space is rather tight, it is also important to minimize the dimensions of the converters. Furthermore, since all the power to the detector will go through these converters which are closely packed, we have to understand the effect of temperature and provide a means of cooling to these devices.

Even with DC-DC conversion, there is concern that the current needed will exceed the ratings of the current power supply modules made by CAEN S.A (Italy). We have contacted the manufacturer to look into ways of modifying the low voltage supply power modules to have a higher rating that can meet our needs. An alternative that we are investigating is to use a two step conversion process. This involves a step-up conversion using commercial parts close to the power supply modules and then a step-down conversion close to the detector.

6.2.7 Front End Electronics

The pixel readout chip used in the current detector (PSI46v2) is well understood, tested. It is also sufficiently radiation hard to survive the Phase 1 integrated luminosity. However, as noted earlier, it will incur rate dependent inefficiencies in the inner regions when the peak instantaneous luminosity exceeds 10^{34} cm^{-2}s^{-1}. Although modifications are needed to allow for the luminosity that we will have for Phase 1 and possible operation with a 50 ns bunch spacing, we would like to keep its core unchanged as much as possible. Changes to the ROC are needed for two reasons:

- **Single hit efficiency:** To cope with the increased luminosity for Phase 1, the size of the internal data buffers must be increased. An additional internal buffer stage on the ROC will be needed which holds the level 1 trigger verified hits until a readout token arrives. Doubling the buffers in the 0.25 μm process will increase the size of the chip periphery by 0.6 mm which can be accommodated in the module design. There is also good progress on designing an improved chip architecture with an additional buffering stage in the column periphery to reduce or eliminate the readout-induced dead time, which limits the efficiency of the innermost layer. This reduces dead time related to readout latency and allows for a more efficient use of the output bandwidth. Simulation shows that for the innermost layer at 3.9 cm, the peak inefficiency of this upgraded ROC at a luminosity of 2×10^{34} cm $^{-2}$s^{-1} is about 4.7% with an average over the whole LHC fill of 2.1%, assuming a fill lifetime of 10 hours, and a collision rate of 40 MHz (25 ns bunch crossing).

DRAFT

- **Fast readout:** Since we will have more modules than the current detector and the number of optical fibers is limited, we need to have a faster readout. The present readout uses 40 MHz analog links, with the pixel addresses encoded using six analog levels (2.5 bits), for an effective bandwidth of 100 Mbps. Increasing the clock rate on the analog links to 80 MHz presents a significant risk due to the limited rise time of the ROC and Token Bit Manager (TBM) signals. Instead, we are developing a digital readout (with an on-chip ADC) from ROC to TBM at 160 MHz (160 Mbps). In addition, a multiplexing TBM combines two token rings into a 320 Mbps digital link, giving three times the throughput of the existing analog links on the same fiber plant. Besides increased bandwidth, advantages of the digital output from the ROC and TBM are lower power and less material in the cables.

The core of the ROC, including the pixel front end amplifier, threshold comparator with trimming and the column drain architecture remain unchanged. A phase-lock circuit (PLL) capable of up-converting the 40 MHz LHC clock to 80/160/320 MHz has been successfully tested. A successive approximation 8-bit ADC has also been tested; revised designs for both PLL and ADC have already been submitted and tested in 2009; further improvements to the ADC for higher clock rates are underway. With these functional blocks designed, laid out and tested, the redesign of the 0.25 μm ROC is on sound footing. The full layout for the upgrade ROC is expected to be ready in Summer 2011, with first test submission following shortly.

In case of a 50 ns bunch crossing scenario of the LHC, the data losses described above would increase by roughly a factor of two. A further reduction of these losses would require modifications to the complex circuit block in the ROC that manages the double column data buffers. Indeed, we intend to pursue such improvements to address readout-related data losses in a follow up submission of the ROC.

Changes are also required to the TBM to accept and produce digital signals. The TBM chip is needed to control a module. The core of this chip will remain largely unchanged. However, modifications will be needed to deal with the new fast up-link protocol. Only modest changes to the input and output stages are required, again using functional blocks already developed for new low-power electrical micro-twisted pair links between the module and downstream electronics. The TBM must also multiplex signals from two token rings run at 160 MHz into a single 320 MHz output to an optical link. The modifications that will be needed include replacing the analog switch drivers by digital multiplexers, a PLL for clock generation, and digital receivers and line drivers.

Digital signals would travel from the TBM on a new set of extremely low mass, flexible cables to an optical hybrid board, and then along optical fibers to the off-detector data acquisition electronics. Micro-twisted pair cable of copper-clad aluminum wires with 125 μm diameter have been developed. On these cables, signals are sufficiently robust over 1 m lengths, to allow the electrical to optical link boards for the barrel to be placed outside the fiducial volume. For FPIX, we are currently evaluating the use of a flat flex-cable made out of Al. Simulation shows good performance when operated digitally at 320 MHz. Prototypes of this cable will be available sometime in early Fall 2010. We are also investigating robust connectors for the both the Al cable and the micro-twisted pair cable.

The current Analog opto-hybrid (AOH) will be replaced with a new readout optical hybrid (ROH) to transmit the data through long fibers to the Front End Driver (FED). The current baseline is to build link boards similar to the existing analog optical hybrids, using 1310 nm lasers qualified for radiation hardness by the CERN Versatile Link project, intended for raw data rates of 5 Gbps, which is well beyond the required 320 Mbps for Phase 1. Several lasers in

DRAFT

commercial TOSA packaging and attached fiber pigtails will be mounted on a common readout link PCB designed to fit in the service cylinders. Prototype lasers and link boards are expected to be available for testing in late 2010. Linear Laser Driver (LLD) chips from the CERN opto-electronics group were used in the original analog links and have been radiation qualified and tested at 320 Mbps. The baseline option is to use the LLD to operate these links at 320 Mbps over approximately 100 m to the FEDs in the Underground Service Cavern, USC55, at CMS where most of the back end electronics is located. A suitable optical receiver has been identified and tested at 320 Mbps.

At the FED, the flash ADC and analog data packet decoder will be replaced by a deserializer, since the incoming signals will be fully digital. The existing FED design has a 9U VME motherboard with daughter cards hosting ADCs or FPGAs for data decoding and event building. One option is to replace the ADC daughter cards with a deserializer FPGA, leaving the architecture of the motherboard intact, where in fact changes are not likely to be necessary. If required, FPGA daughter cards can be replaced with faster FPGAs from the current generation of devices from Altera. A preliminary design for the replacement cards includes an extension for mounting the new optical receivers, leaving the old analog receivers intact. This may prove useful for prototyping and conversion of existing FEDs for digital readout. To accommodate the increased data rates at the FED output, the existing S-Link64 interface cards on the VME mezzanine boards would be replaced with new daughter boards implementing a new interface to the CMS DAQ system.

The downlink protocol for control and configuration of the detector is unchanged, both electrically and logically. New parts have to be procured for the digital control links and Front End Controller (FEC).

6.2.8 Sensor Module

A 4-layer barrel detector would comprise about 1200 full modules compared to the presently installed 770 full and half-modules. The number of pixels grows by a factor 1.7 from 48M to 80M. There are 672 modules in the upgraded 2×3-disk forward pixel detector, the same number as the current FPIX detector. However, since the size of each module will be larger, the number of pixels will grow from 18M to just under 45M.

The proposed upgraded pixel detector has only one type of sensor module with two rows of 8 ROCs each. This will simplify considerably the sensor production, module assembly, and testing. The active area of the module is 16.2 x 64.8 mm^2. The pixel size will remain the same as before, 100 x 150 μm^2. For the sensors our baseline is to use the same n^+-on-n technology as for the current detector. Nevertheless, there is some ongoing R&D activity to evaluate other radiation tolerant sensor technology. The sensor is bump-bonded to 16 ROCs which for Layers 1 and 2 for BPIX, will be thinned down to 75 μm. For the rest of the layers and the end-cap disks, the ROCs will be thinned down to about 200 μm. A high density interconnect (HDI) is glued on top of the sensor with wire bond pads to connect to the corresponding pads on the ROCs. Electrical signals will be sent from/to the ROCs through the HDI and then to the downstream electronics. The TBM chip will be mounted on the HDI as well. A small clip is glued to the ends of the module to allow the assembly of the module to its support structure.

For future replacements of the the detector innermost layers and rings we are considering other possibilities as outlined in Section 6.4.

DRAFT

6.2.9 Bump bonding

Bump bonding was a cost and schedule driver for the current pixel detector [8]. Since the number of pixels of the upgraded pixel system will increase by about 90%, some development work will be needed to increase the throughput as well as reduce the cost. For the current BPIX detector, bump bonding was done by PSI whereas for FPIX by two industrial companies. Industry is progressing steadily on bump bonding and lower cost processes for micro-bumps at 30 μm diameter and 100 μm pitch are becoming available. For example, at PacTech [9], prefabricated solder balls are individually placed through a capillary and fused by laser-melting at a speed of 5–10 per second on a step-motor controlled machine. A special under-bump metal is still required, but the processing steps for the deposition and forming of Indium balls can be omitted. Any new vendor and process will have to be qualified to make sure that they meet our needs. In addition, the production yield and throughtput must be evaluated in a sequence of prototype runs.

6.2.10 Pixel Module Assembly and Testing

Starting from the bump-bonded pixel module, a high density interconnect will be glued onto the back of the sensor and wire bonded to the readout chips (about 700 bonds per module). Production of the necessary gluing and placement tools, based on assemblies used to build the current detector, has started. These assembly stations will include both manual and automatic procedures. The design and testing of fixtures, adhesive dispensing machines, and the necessary software are being commissioned.

Once assembled, the full modules then have to be fully tested and characterized at room temperature and at the foreseen operation temperature around -20°C. The tests include trimming the analog thresholds of all of the pixels to achieve uniform efficiency. The pixel detector achieves a point resolution of about 10 μm with 100 μm pitch by using the charge sharing induced by the Lorentz effect. The amplification is non-linear for small pulses and needs to be calibrated for each pixel using X-ray sources between 10 and 30 keV to reach the design resolution. The modules should also be tested at high rate, which can be done using an X-ray test stand.

In BPIX the final modules of one layer have to be mounted on a carbon-fiber frame which also includes the cooling pipes. A rotating fixture is needed, as adjacent ladders are mounted alternating from the inside and outside.

A system test of the fully assembled layer would require a CO_2 cooling plant of about 1kW, HV and LV supplies, optical links, control and readout boards, and a cosmics trigger.

6.2.11 Final integration and commissioning

Our plan is to do the final integration followed by system commissioning in the Tracker Integration Facility (TIF) at CERN. For BPIX, fully assembled layers will be transported from the various assembly sites to CERN. For FPIX, completed half disks and half cylinders will be shipped separately to CERN. At TIF, we will re-mount the half-disks to the half cylinders and carry out a commissioning of each half cylinder. Finally, extensive system tests of both BPIX and FPIX together will be performed at TIF prior to installation in CMS. 9 months are scheduled for this phase to minimize further commissioning in CMS for physics operations

A program of high rate tests will be performed to uncover issues with the interoperability of the readout chain. This system test will allow us to exercise all firmware and software in the system. Cooling system tests will be performed to assure smooth, leak-free operation. In

DRAFT

preparation for these tests, we will equip TIF with all the necessary electronics, power supply modules, as well as a CO_2 cooling system. The full readout and data acquisition chain will be present. We will also have a full control and safety system (DCS/DSS) installed and tested.

6.3 Performance Studies

The Phase I pixel detector has significantly reduced mass and significantly increased three-hit coverage. The net effect of these improvements on the amount of material, pattern recognition, track parameter resolution, vertexing, and b-tagging performance of the Tracker is summarized in the following sections.

6.3.1 Studies of the Effects of Material in the Tracking Volume

The upgraded detector will roughly double the number of pixels in the system. Despite this, we aim to reduce the amount of material in the tracking region by at least a factor 2 with respect to the current system.

The amount of material from the barrel pixel detector can be significantly reduced both in the active regions and even more in the service regions located in front of the pixel disks and the silicon strip tracker [10]. The use of serial CO_2 cooling with reduced density and pipe wall thickness is one important ingredient. This will reduce multiple scattering, photon conversions, and nuclear interactions. Within the region $|\eta| < 2.1$, the weight of the supply tube is 408 g and the total weight of the 4 barrel layers plus supply tube within this η region is estimated to be 7 kg, about a factor 2.4 less than the current BPIX detector with only 3 layers.

We estimate the overall mass of the FPIX detector can be reduced by $\sim$ 40%. The half disks contribute most to the FPIX material in the region $1.5 < |\eta| < 2.5$. It is feasible to remove 50% of the mass in the half disk by removing the very high density interconnect circuit (VHDI) and by using CO_2 cooling. The weight of the new half-disk is estimated to be 420 g, to be compared with the present 607 g. Within $|\eta| < 2.5$, the total weight of each half cylinder, including the three half-disks, cables, and cooling lines, is estimated to be 1.82 kg.

These reductions in material inside the pixel tracking volume are shown in Figure 6.17 and Figure 6.18 for BPIX and FPIX, respectively.

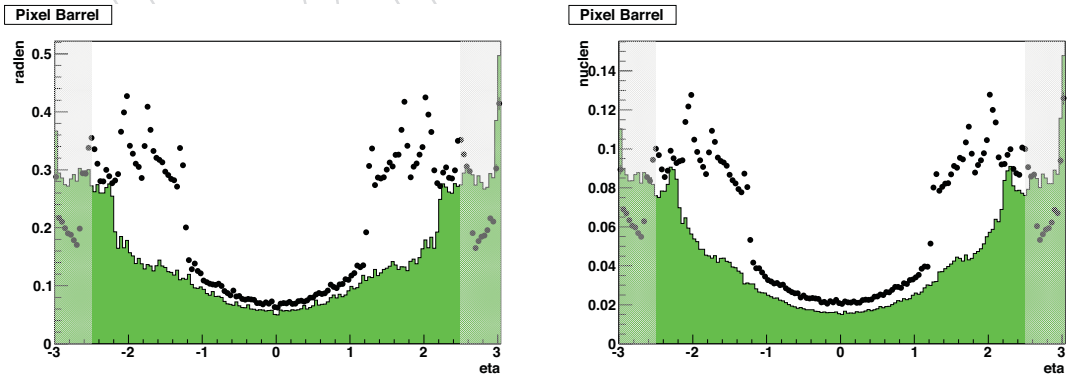


Figure 6.17: Radiation length (left) and nuclear interaction length (right) of current barrel pixel detector (dots) and proposed upgrade (histogram). The shaded region shows the material distribution outside the fiducial tracking volume.

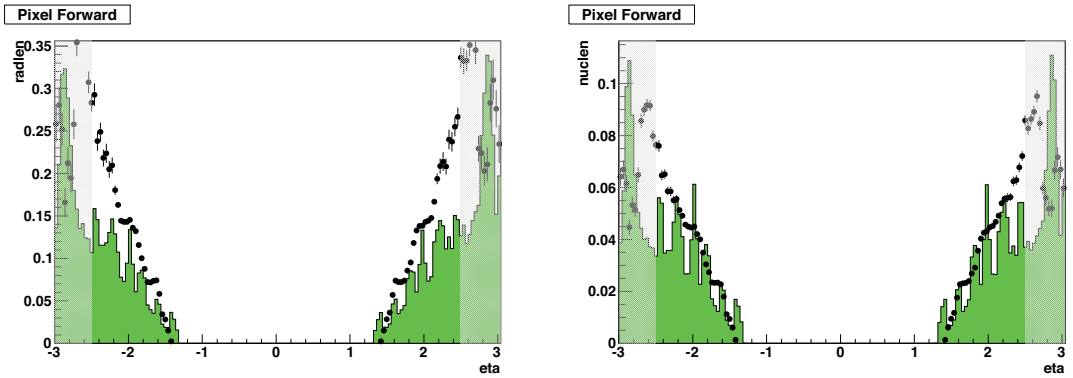


Figure 6.18: Radiation length (left) and nuclear interaction length (right) of current forward pixel detector (dots) and proposed upgrade (histogram). The shaded region shows the material distribution outside the fiducial tracking volume.

Such reductions in the amount of passive material will have a large impact on charged particle tracking efficiency as well as electron and photon identification and resolution. For example, for a photon at $|\eta| = 1.5$, the probability that it would convert into an electron-positron pair inside the pixel volume (where the presence of pixel hits is crucial for distinguishing photons from electrons) is 22% with the current detector, but would be 11% with the proposed upgraded detector. Such improvements would have a positive impact on final state signatures involving photons, such as $H \rightarrow \gamma\gamma$.

6.3.2 Pattern Recognition and Efficiency Studies

The number of overlapping events during Phase 1 operation will be two to four times larger than during previous LHC operation. The interesting physics to be pursued during Phase 1 is likely to involve the reconstruction of tracks in high-p_T jets. These realities will emphasize the importance of reliable tracking in environments with high local hit densities. The challenge of maintaining high tracking efficiency and low track fake rate in dense hit environments has been studied as part of the CMS heavy ion program. It was found that seeding with three-hit combinations in the pixel detectors results in more precise initial estimates of the track parameters, which produces more reliable identification of the associated silicon strip hits and lower fake rates. Unfortunately, due to module boundary gaps in the current pixel detector with three barrel layers and two disks, this requirement leads to losses in efficiency. The new design with four barrel layers and three disks alleviates this problem by providing substantial redundancy for three hit seeds. The fourth layer also guarantees at least reasonable track seeding after high integrated luminosity. With four layers, even if the inner layer performance starts to degrade, the fourth layer will still provide three layer seeds.

In order to quantify the physics benefit that can be expected from the upgraded pixel detector, samples of jet events and $t\bar{t}$ events were generated for both geometries using the standard CMS simulation software and assuming an instantaneous luminosity of 2×10^{34} cm^{-2}s^{-1}. CMS has adopted an iterative tracking algorithm consisting of multiple steps. In the first step, hit triplets from the pixel detector or the innermost strip layer are used as seeds for the subsequent track finding and fitting. With the upgraded detector, in addition to triplets, quadruplets of pixel hits can also be used which cleans up the subsequent pattern recognition and reduces the fake rate. The left-hand plots of Fig. 6.19 show the track finding efficiency for the two geometries as a function of pseudorapidity and p_T. The track selection criteria are the same ones used in the recently released tracking performance studies [7] and represent the typical

requirements used in recent physics analyses. The redundancy provided by the additional pixel layer in the Phase 1 geometry results in an increase of track seeding efficiency and a much lower fake rate. Losses due to nuclear interactions in the tracker material, which presently increases from about 0.4 X_0 in the central region to 1.8 X_0 at $|\eta| = 1.5$ (see Figure 6.7), and which is dominated by dead material of the strip detector, lead to a significant drop of efficiency towards the acceptance limits of the barrel pixel detector. The comparison of the tracking efficiency in the two configurations demonstrates however that the gain in track seeding efficiency can be retained also for physics analyses.

The plots on the right-hand side of Fig. 6.19 show the corresponding fake track rate as a function of pseudorapidity for the current and Phase 1 detectors. Fake tracks are caused by the incorrect association of hits and are much more likely in regions with more passive material. They cause significant problems for b-tagging and are much reduced in the upgraded detector.

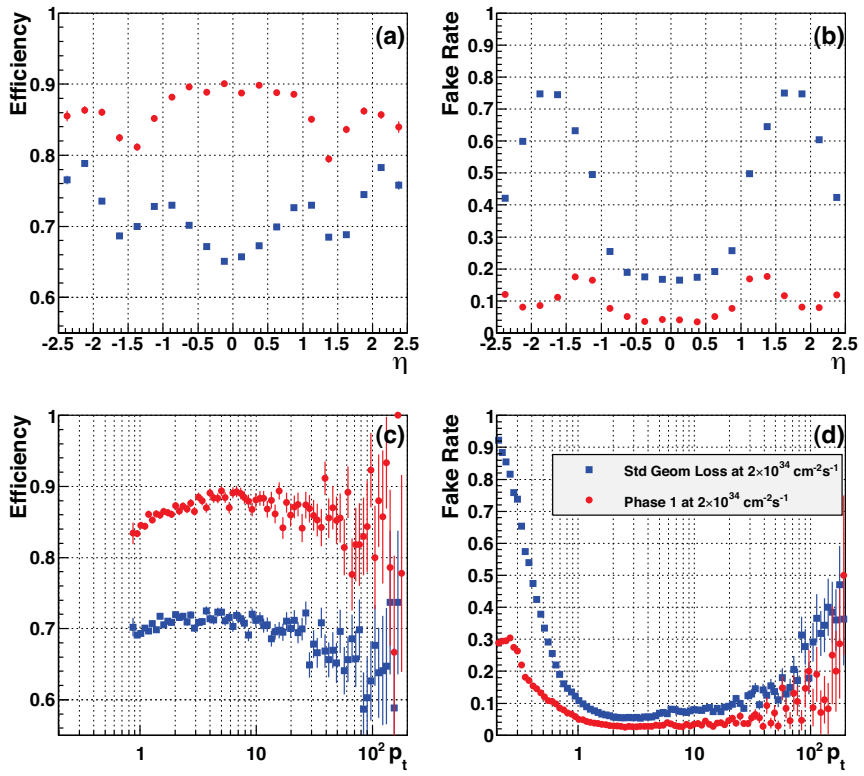


Figure 6.19: Comparison of tracking efficiency and fake rate for the current (blue) and upgraded (red) detectors in $t\bar{t}$ events at $2 \times 10^{34}\,\mathrm{cm}^{-2}\mathrm{s}^{-1}$ with 25 ns bunch spacing. The tracking algorithm with the current detector uses pixel triplets to seed pattern recognition, and pixel quadruplets and triplets with the upgraded detector. Shown are: (a) tracking efficiency vs pseudorapidity; (b) fake rate vs pseudorapidity; (c) efficiency vs p_T; (d) fake rate vs p_T.

6.3.3 Track Parameter Studies

The primary purpose of the pixel detector is to make precise measurements of the track direction and position before that information is degraded by multiple scattering. The increased sampling and reduced mass of the Phase 1 pixel detector also improve the track parameter resolution. The full-track impact parameter resolutions for the current detector and for the Phase 1

upgrade are shown as functions of pseudorapidity and momentum in Figures 6.20-6.21. Substantial improvement to the impact parameter resolution is a result of four main factors:

1. Reduced material in the tracking volume which reduces multiple scattering;
2. Moving the innermost layer closer to the interaction region;
3. Adding a fourth layer to the BPIX and a third disk to the FPIX which improves the track "lever arm" in the pixel region;
4. Improving the transverse impact parameter resolution in the forward regions by orienting the pixel sensors so that the 100 μm pitch (as opposed to the 150 μm pitch) contributes to the FPIX cluster resolution in the transverse plane.

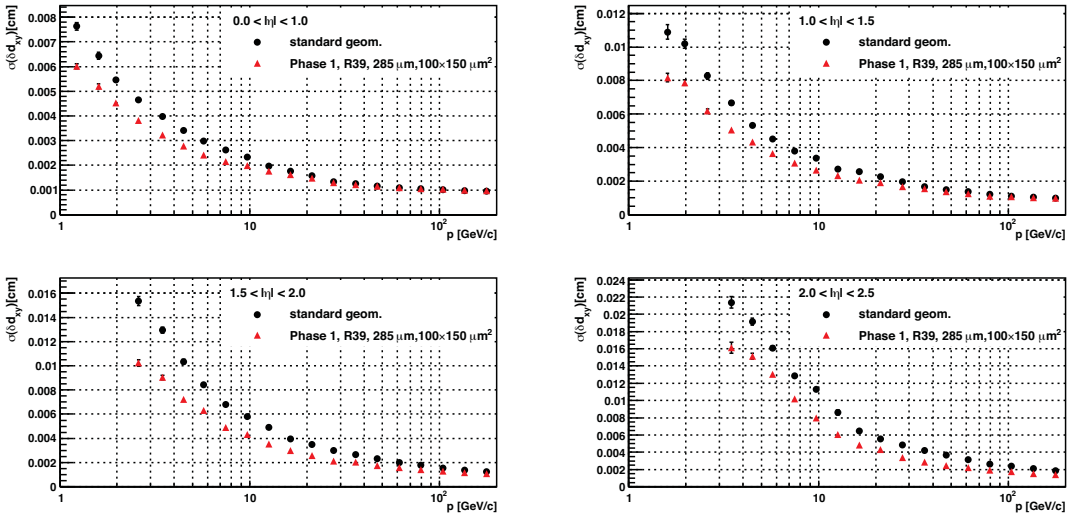


Figure 6.20: The transverse impact parameter resolution for the present and upgraded versions of the pixel detector as functions of track momentum in different pseudorapidity regions.

As a consequence, vertex resolution and b-tagging performance also improve, as described in the following sections.

The addition of a fourth barrel pixel layer increases the measured radial track length by a factor two, thus improving the momentum resolution for stand-alone pixel tracks by a factor four. This improves both the seeding and the extrapolation into the first layer of the strip tracker, and provides more powerful information to the HLT.

6.3.4 Vertex Resolution Studies

One of the primary functions of the CMS Tracker is to reconstruct primary and secondary vertices. It is expected that the Phase 1 detector will operate in an environment with a mean of 20-40 pp interactions per bunch crossing. Efficient and precise vertexing and the efficient association of individual tracks to vertices are essential to untangle the accidental coincidences of less interesting event topologies that could otherwise appear to signal important discoveries. The efficient and precise reconstruction of secondary vertices is a crucial element in b-tagging and in the search for possible long-lived exotic states. The longitudinal and transverse resolutions of simulated primary vertices are shown in Fig. 6.22 as functions of the number of

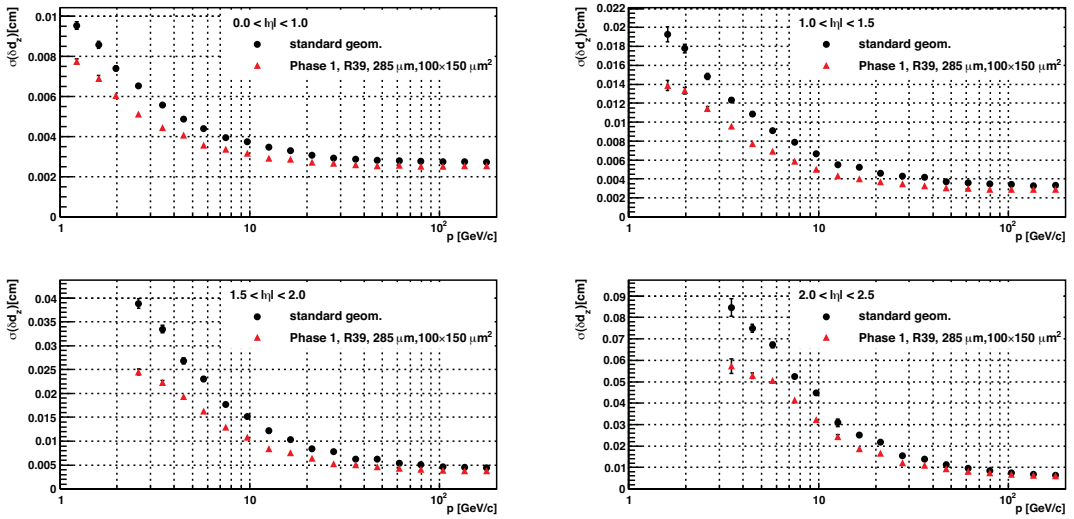
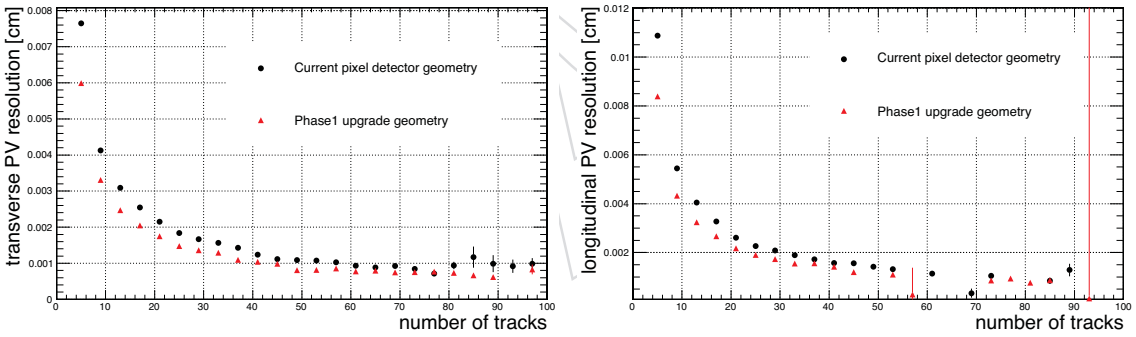


Figure 6.21: The longitudinal impact parameter resolution for the present and upgraded versions of the pixel detector as functions of track momentum in different pseudorapidity regions.

tracks for the present detector and for the upgraded detector. Overall, the upgrade gives an improvement in the resolution of about 20%.



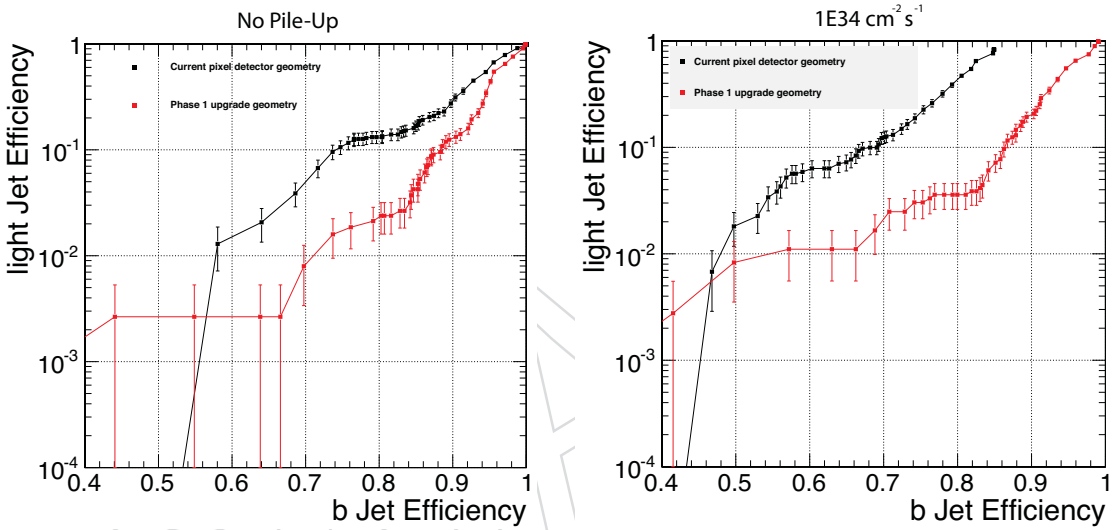
(a) (b)

Figure 6.22: The (a) transverse and (b) longitudinal primary vertex resolutions for the present and upgraded versions of the CMS pixel detector as functions of number of tracks in simulated $t\bar{t}$ events at $10^{34}\text{cm}^{-2}\text{s}^{-1}$.

6.3.5 *b*-tagging Studies

A number of interesting physics channels such as top quarks, Higgs bosons, and supersymmetric particles produce b jets in the final state. For example, a low mass Standard Model Higgs boson dominantly decays into a pair of b quarks, while the top quark decays almost exclusively into a W boson and a b quark. Various supersymmetric scenarios can produce final states with four or more b quarks. The efficient and pure identification of b jets is therefore a major element in the CMS physics program. The identification of b jets relies upon the relatively distinct properties of b hadrons such as large proper lifetime ($\tau \approx 1.5$ ps, $c\tau \approx 450$ μm), large mass, decays to final states with high charged track multiplicities, relatively large semileptonic branching ratios, and a hard fragmentation function. Efficient track reconstruction, and in particular pre-

cise spatial reconstruction close to the interaction point, are thus key ingredients for almost all b-tagging algorithms. The performance improvements provided by the Phase 1 upgrade also enhance the b-tagging performance as shown in Fig. 6.23 for a sample of simulated (QCD) multijet events with transverse momenta in the range 80-120 GeV/c. Fig. 6.23a shows the detector performance for low instantaneous luminosity and Fig. 6.23b shows the performance for operation at an instantaneous luminosity of 10^{34} cm^{-2}s^{-1} with 25 ns bunch spacing. The b-tagging performance of the present detector is seriously degraded by the large number ($\sim$20) of overlapping interactions in each bunch crossing. The upgraded detector would reduce the light quark background of the Combined Secondary Vertex Tag by more than a factor of 6 for a b-efficiency of 60% or conversely, it would increase the b-efficiency by 50% at the fixed light-quark efficiency of 5×10^{-2}. The search for new physics frequently involves the identification of multi-b-quark final states. These searches would benefit by a factor of $(1.5)^n$ where n is the number of final state b quarks.



(a) (b)

Figure 6.23: The b quark efficiency of the Combined Secondary Vertex Tag is plotted versus the light quark (and gluon) efficiency for a sample of dijet and multijet events of transverse momenta in the range 80-120 GeV/c. The black points represent the performance of the current tracker and the red points represent the performance of the Phase 1 upgrade. (a) The instantaneous luminosity is assumed to be low enough that there are no multiple collisions. (b) The instantaneous luminosity is assumed to be 10^{34} cm^{-2}s^{-1} with 25 ns bunch spacing.

6.4 Further development for the innermost region

The innermost region of the pixel detector is expected to suffer degradation when the LHC reaches its high luminosity running in the later stages of Phase 1. The inner layers and rings have been designed, as described above, to be independently replaceable. An R&D line should continue for new detector modules with smaller pixel size and other enhanced features. The most important improvements target the module efficiency, radiation-hardness, and spatial resolution, aiming not only at better performance, but also more headroom relative to LHC conditions, or radiation backgrounds, which could exceed our expectations. The new modules

must remain fully compatible with the rest of the Phase 1 mechanics, cooling and electrical systems.

6.4.1 Frontend electronics and sensors

Development of a new ROC is under consideration using CMOS technology of 130 nm or smaller. This will enable the engineering of a module with a smaller pixel size and lower readout thresholds. This will result in better spatial resolution and better ability to resolve tracks inside high momentum jets, where the present pixel size leads to overlapping hits in jets of energy above 100 GeV. The new ROC should also be able to operate with high efficiency with LHC operating conditions up to $2 \times 10^{34}\,\mathrm{cm}^{-2}\mathrm{s}^{-1}$ and 50 ns bunch separation.

The replacement of the innermost layers and rings also constitutes an opportunity to adopt sensors with greater radiation hardness. Recent measurements shown in Figure 6.24 show that sensors processed on mCz silicon collect the same signal at a lower bias voltage than those processed on FZ material. We are currently evaluating n-on-n and n-on-p single-chip pixel

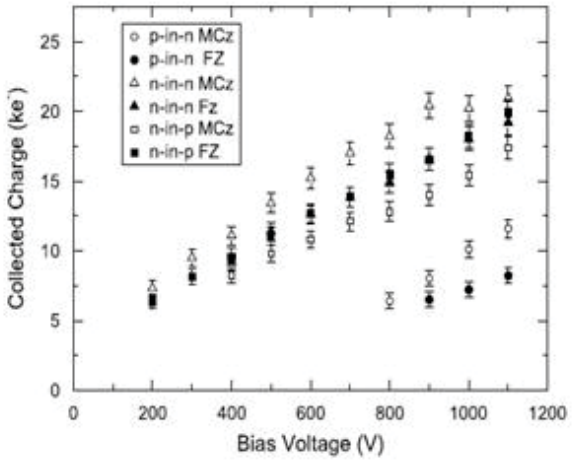


Figure 6.24: Collected charge as a function of bias voltage for six types of sensors irradiated with neutrons to $10^{15}\mathrm{n_{eq}}/\mathrm{cm}^2$ [11]

detectors processed on FZ, DOFZ and mCz material from different producers. A small number of n-on-p samples of FZ and mCz are available from Micron, IRST and CiS. A larger quantity of samples produced on different wafer types (FZ, mCz, epi) of different thickness and technology (n-in-n and n-in-p with p-stop and p-spray isolation) has been delivered recently by HPK and Sintef. Other options under consideration include the development of non-planar (so called 3-D) and diamond sensors.

6.4.2 Performance studies

The development of a readout chip with higher granularity and lower readout thresholds would offer the opportunity for further improving the detector later in Phase 1 in several key aspects:

- Enhanced hit resolution and detection efficiency after irradiation;
- Improved track parameter resolution;
- Improved jet reconstruction and b jet identification.

The pixel hit resolution is determined by the cell size, the charge sharing due to the combined effect of electric and magnetic fields, and by the readout threshold. The resolution can be improved by adopting pixel cells with smaller dimensions and front end electronics with lower readout thresholds. Figure 6.25 shows the hit resolution after irradiation for a hypothetical scenario with a smaller pixel cell size, thinner sensors (220 μm) and lower readout thresholds (2000 electrons). We are considering further R&D on CMOS frontend electronics and sensors

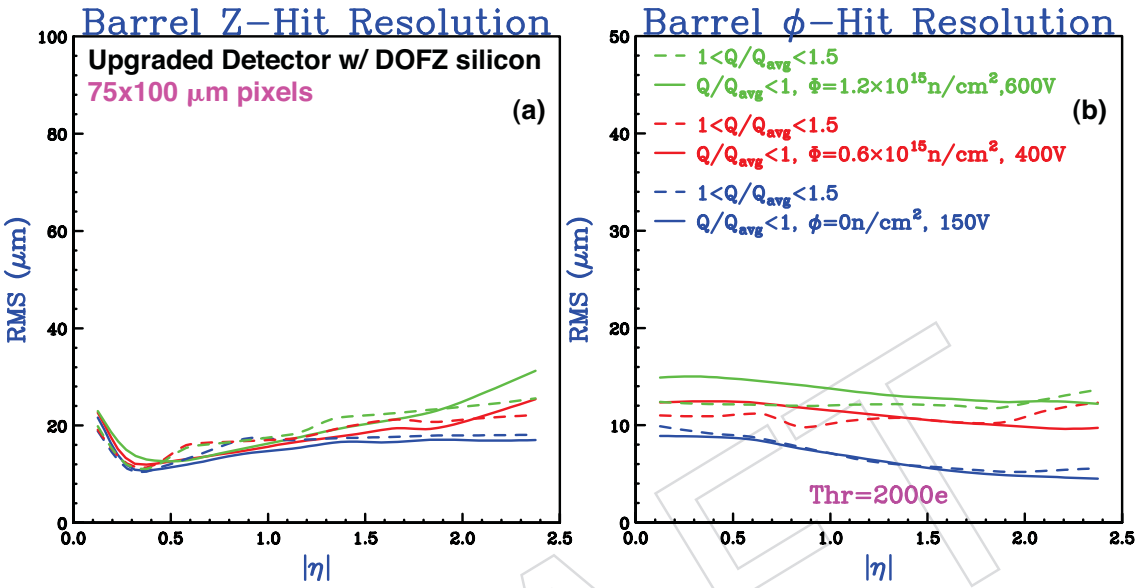


Figure 6.25: Hit position resolution (RMS) as function of the track pseudorapidity for an unirradiated (blue lines) and irradiated detectors (red and green lines). The pixel cell size is set to 75 $\times$ 100 μm^2 and the sensor thickness to 220 μm. (a) Longitudinal and (b) transverse hit resolution are shown separately. The solid lines correspond to hits with total charge Q below the average charge. Dashed lines correspond to hits with total charge $1 < Q/Q_{avg} < 1.5$.

in these directions.

At large momenta, the resolution on the track impact parameters and angles are largely determined by the hit resolution and radius of the innermost layer, and precision of the spatial alignment. For instance, with a hypothetical pixel cell of 75$\times$100 μm^2 in the 39 mm radius innermost layer, the longitudinal impact parameter resolution could be improved by 25%, as shown in Figure 6.26. Additional small improvements can be expected by further reducing the radius of the innermost layer. However, any reduction with respect to the baseline radius would require a careful assessment of the risks associated to the clearances during installation.

Primary and secondary vertex resolution is largely determined by the number of tracks associated to the vertex and resolution of track parameters. However, the hadronization of b quarks with large transverse momentum produces collimated jets which result in overlapping hits in the innermost pixel layer. In the current detector, for a 200 GeV b jet about 20% of the tracks have merged hits in the first layer. The effect produces a sizable deterioration of the b jet identification for jets with transverse momenta above 200 GeV. Future replacements of the innermost layer with sensors featuring smaller cell sizes, therefore, represent an opportunity to improve b jet identification in this upper kinematic range.

DRAFT

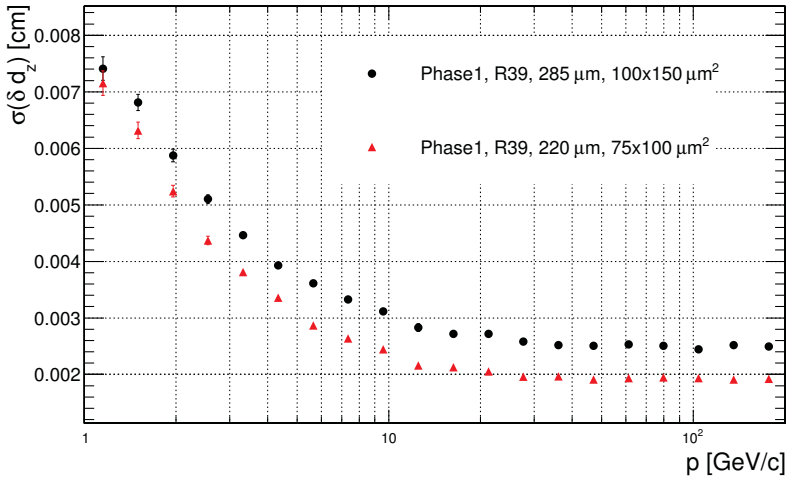


Figure 6.26: Longitudinal impact parameter resolution for the baseline upgrade scenario (black dots) and with a hypothetical replacement of the innermost layer adopting a reduced pixel cell size (red triangles).

6.5 Schedule

Figure 10.3 shows a tentative schedule for the Phase 1 pixel upgrade.

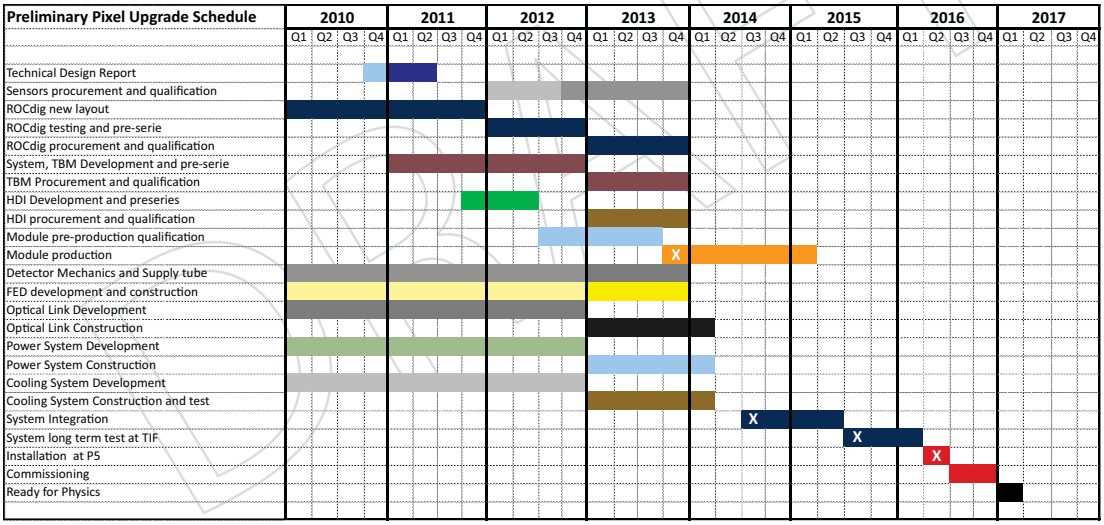


Figure 6.27: Tentative schedule for the Phase 1 upgrade pixel detector.

6.6 Conclusions

The Phase 1 upgrade of the LHC, starting with the long shutdown in 2016, presents CMS with both the requirement and the opportunity to upgrade the present pixel detector. The peak LHC luminosity after the Phase 1 upgrade is expected to reach up to 2×10^{34} cm^{-2}s^{-1} with a possibility of 25 ns or 50 ns bunch spacing. Such conditions are a factor two to four more intense than the nominal LHC conditions for which the present pixel detector was designed. The present system with its three-hit layout would suffer greatly in terms of performance in these

conditions, severely compromising the ability of CMS to fully exploit the delivered luminosity from the upgraded LHC.

A thorough revision of the design of the ROC has been made, aiming to reduce the dynamic inefficiency to an acceptable level, while leaving the underlying architecture unchanged. So far, a large reduction of inefficiency has been achieved with the new design, and effort will continue towards further reducing the data loss. The bandwidth of the readout has been doubled in the new design allowing the much larger system to be read out with the same number of fibers.

The addition of extra barrel and endcap layers will preserve our present excellent level of tracking performance even at the higher luminosity expected in Phase 1. Recent advances in CO_2 cooling, DC-DC powering, and readout links enable this ambitious proposal for the complete replacement of the present three-hit pixel system with a much larger ultra-lightweight system of four barrel layers and three endcap disks. The upgraded pixel system will have a reduced mass, a reduced innermost radius and increased lever arm, altogether resulting in a significant improvement over the present system in terms of tracking, vertexing and b jet identification.

Radiation effects will be of growing importance as the luminosity increases. The innermost detectors are expected to require replacement before the end of Phase 1 LHC operations. Such an intervention can be done during an LHC winter maintenance period. This replacement of the innermost layers presents a further opportunity to improve the detector performance at a later stage. Long term R&D is being done with the objective of having available sensors with greater radiation resistance. We are also considering designing a new readout chip in a more advanced CMOS technology, aiming to enhance the performance in terms of hit-efficiency and threshold, while also profiting from the potential to employ a smaller pixel size. There is a clear synergy here with R&D required for Phase 2 upgrade of the full Tracker system, which is also the case for the R&D on CO_2 cooling, power and readout systems.

The new system has to be commissioned and ready to take good physics data very soon after installation. The proposed schedule is compatible with having the detector integrated well in advance of the installation date, allowing time for extensive system tests at CERN and commissioning of large parts, if not the entire detector, prior to installation.

DRAFT

DRAFT